TECHNICAL REPORT NO. 6

To

The Office of Naval Research
Contract No. N00014-91-J-1414

MECHANISMS OF FRACTURE AND CREEP OF STRUCTURAL ALLOYS

D. A. Koss

Department of Materials Science and Engineering
The Pennsylvania State University
University Park, PA 16802

Annual Report for the period
1 January 1992 - 28 February 1993

REPORT DOCUMENTATION PAGE

Form Approved
OMB No. 0704-0188

1. AGENCY USE ONLY (Leave blank)	2. REPORT DATE	3. REPORT TYPE AND DATES COVERED
	March 29, 1993	Annual Report: 1/1/92 - 2/28/93

4. TITLE AND SUBTITLE

Mechanisms of Fracture and Creep of Structural Alloys

5. FUNDING NUMBERS

6. AUTHOR(S)

D. A. Koss

7. PERFORMING ORGANIZATION NAME(S) AND ADDRESS(ES)

Dept. of Materials Science and Engineering
The Pennsylvania State University
University Park, PA 16802

8. PERFORMING ORGANIZATION REPORT NUMBER

Report No. 6

9. SPONSORING/MONITORING AGENCY NAME(S) AND ADDRESS(ES)

Office of Naval Research
800 N. Quincy Street
Arlington, VA

10. SPONSORING/MONITORING AGENCY REPORT NUMBER

11. SUPPLEMENTARY NOTES

12a. DISTRIBUTION/AVAILABILITY STATEMENT

Distribution of this document is unlimited.

12b. DISTRIBUTION CODE

13. ABSTRACT *(Maximum 200 words)*

Progress is reviewed for a research program which focuses on two aspects which limit the performance of structural alloys. First, in a study generic to a wide range of materials, we are determining the mechanisms, as well as local failure criteria, by which voids grow, interact and link during ductile fracture due to damage accumulation. Secondly, in a study focused specifically at high strength titanium alloys, we are examining the deformation and fracture behavior of novel beta titanium alloy Ti-23Nb-11Al, which is age-hardenable by the formation of ordered precipates based on Ti_3Al. Progress for the period January 1, 1992 to February 28, 1993 is reviewed for the following projects:

(1) two-dimensional modeling studies of void linking during ductile, microvoid fracture
(2) a three-dimensional experimental modeling study void growth and linking during ductile fracture, and
(3) the influence of temperature on the deformation and oxidation behavior of a new age-hardenable beta titanium alloy.

14. SUBJECT TERMS

Tensile Fracture, Void Growth, Void Linking Beta Ti Alloys, Deformation, Fracture, Oxidation

15. NUMBER OF PAGES

33

16. PRICE CODE

17. SECURITY CLASSIFICATION OF REPORT	18. SECURITY CLASSIFICATION OF THIS PAGE	19. SECURITY CLASSIFICATION OF ABSTRACT	20. LIMITATION OF ABSTRACT

INTRODUCTION

The performance of advanced structural systems depends critically not only on the strength and fracture behavior of the component materials but also on our ability to predict the behavior. Thus, accurate computational models must exist for predicting mechanical performance, especially fracture, not only under a range of service conditions but in terms of the critical microstructural features. The present program addresses the damage accumulation form of tensile fracture by studying the manner in which voids (or pores) control the ductile fracture of structural alloys. In an unique, very fundamental approach, this study utilizes a combination of experimental modeling and computational analyses which establishes the mechanisms, as well as local failure criteria, by which voids or pores grow and link during ductile, microvoid fracture. Both two-dimensional and three-dimensional modeling studies are being performed. The results should not only extend existing fracture theories but also provide a basis for intelligent microstructural control of structural alloys by improved materials processing and design. This effort requires an integration of materials and mechanics efforts; as such, the research relies on the active participation of Dr's. Peter Matic of the Naval Research Laboratory and Michael Stout of the Los Alamos National Laboratory. Two graduate students have been involved in this aspect of the research program: Andy Geltmacher, a Ph.D. candidate, and Luis Forero, a Fulbright Scholar who recently completed a M.S. degree and has returned to the faculty of University of Industrial de Santander in Columbia, South America.

The second aspect of the present research program has focused on a specific alloy system. We recognize that most commercial beta Ti alloys are age hardenable due to the formation of disordered hcp alpha-phase particles in the 450°-500°C range. Thus, the use of existing beta Ti alloys in a strengthened condition is necessarily limited to relatively low temperatures. As part of this ONR program, we have recently shown, for the first time ever, that it is possible to age harden the beta Ti alloy Ti-23-Nb-11Al (at %) with ordered alpha-two precipitates based on Ti_3Al. Hardness data indicate that it is possible to age harden the alloy at temperatures as high as 675°C, or nearly 200°C higher than is possible with conventional beta alloys. Furthermore, the room

temperature yield strength of specimens aged to peak hardnesses are quite impressive; yield strengths of 1700 MPa have been obtained for specimens aged at 575°C with no alloy development. As will be described later, the most recent part of this investigation has examined the influence of temperature on the deformation and oxidation behavior of the Ti-23Nb-11Al alloy. Present efforts are focusing on the room temperature ductility response, especially under conditions of high strength. This research is being conducted by Dana Goto, who just completed his M.S. degree and may continue for the Ph.D.

A significant impact of this research is the quality of the educational experience derived by the graduate students involved. The fracture aspect of this program is designed to foster an understanding and appreciation of both materials and mechanics aspects of fracture in the Geltmacher-Forero studies and to require interaction between the student (Geltmacher) and national laboratories [Naval Research Laboratory and Los Alamos National Laboratory]. The titanium project requires the student (Goto) to become involved in, and understand, a wide range of properties [low temperature fracture and strengthening behavior, intermediate temperature flow instabilities, high temperature creep and oxidation behavior] which limit the use of high temperature structural alloys.

VOID GROWTH AND LINKING DURING DUCTILE FRACTURE

1. Background

The nucleation, growth, and linking of voids are critical in the ductile fracture of commercial alloys and particulate-reinforced metal matrix composites. Void growth has been theoretically modeled by several investigators. Rice and Tracey initially examined the growth of isolated spherical voids.[1] Subsequent computational analyses using the finite element method (FEM) have verified the Rice-Tracey analysis for both non-linear viscous[2] and strain-hardening materials.[3] However, serious problems arise when these analyses, which are based on the growth of isolated voids, are used to predict the fracture behavior of materials. For example, the predicted uniaxial ductilities based on the growth of isolated voids to impingement are much larger than those

experimentally observed.[4] Clearly, void interaction effects must be important in determining the fracture behavior of structural alloys.

Attempts to incorporate void interaction effects have been done analytically and computationally by modeling cavities as either cylindrical holes or spheres in a material subjected to uniaxial tension[4-8] or near a blunting crack tip.[9,10] However, no direct experimental validation is offered. These analyses predict strong void-void interaction effects under a strongly triaxial state of stress, but no significant interaction in uniaxial tension.[6] Thus, predictions of uniaxial ductility based on stable void growth to impingement and coalescence retain the same problem as the isolated-void analyses; the predictions grossly overestimate tensile fracture strains. Furthermore, this lack of agreement with experimental tensile ductility data calls into question the accuracy of the analyses of the void growth and coalescence behavior ahead of a blunting crack,[9-10] which is a cornerstone for understanding certain fracture toughness phenomena of structural materials.

An alternate approach to void linking is to hypothesize that void interaction effects are much stronger than that predicted by FEM. This could result in a rapid, strain-induced decrease of ligament width and accelerated void coalescence (even during uniaxial tension), perhaps promoting a load instability within the ligament.[16] As mentioned earlier, FEM computations for voids spaced one diameter apart predict strong void interactions only under highly triaxial states of stress.[6] The next section will show this prediction is wrong; our experiments show significant void interaction effects occur even under uniaxial tension at one void diameter spacing. This implies that accelerated void coalescence may occur in uniaxial tension; thus, we may not have to rely on arbitrarily geometric linking criteria in order to obtain agreement between theory and experiment on porous materials. Furthermore, the above lack of experimental validation of existing computational predictions calls into question their accuracy regarding void growth and coalescence near crack tips.

A second possibility which also results in accelerated void linking is based on the notion that the presence of voids induce plastic instabilities, which localize flow onto planes of high void content and triggering fracture. The void-sheet type of failure is a good example. Analyses of this

form of void-induced fracture have been performed on a continuum basis usually by assuming the pre-existence of long, weak bands of material containing locally high densities of voids[11-13]. Under certain plasticity conditions these weak bands ("imperfections") can develop into a form of localized necking. While appealing conceptually, such a microstructural imperfection is very hard, perhaps impossible, to quantify. A much different analysis is based on two-dimensional modeling experiments in which hole linking is a step wise process in which closely spaced holes link, concentrate strain, and promote the evolution of a plastic instability[14-15]. This analysis begins with a pseudo-random hole/void microstructure, and accounts for void clustering. However, computational predictions based on this model are very sensitive to the concentrations of strain near groups of voids and require a well-defined ligament failure criterion. The previous research[15] in this regard was limited to experimental characterization of strain distributions for two specific materials (Al and brass) between pairs of holes under conditions of plane stress. Despite these severe limitations, computational predictions of uniaxial failure strains were in reasonable agreement with experimental data[15]. However, for this approach to predict fracture accurately, and in a more general manner, the influence of material parameters, such as strain hardening, and mechanics of loading, such as stress state, must be addressed.

Our current research addresses both of the above issues. The next section describes our current efforts to conclude our two-dimensional modeling research by using a combination of experimental and computational analysis to examine strain evolution and the development of hole linking by plastic strain concentration in specimens containing pseudo-random arrays of holes, and subjected to either uniaxial or equal-biaxial tension. Computational analysis is also performed in order to indicate the influence of strain hardening on strain concentrations near holes and hole linking. In the subsequent section, preliminary results from a three-dimensional experimental study of void growth and linking will be described. The experiments, which are unique, describe the void growth behavior of neighboring cavities and identify significant void-void interactions effects not predicted by computational analysis.[6] These results contain significant implications to fracture dictated by void (or pore)-induced strain localization phenomena.

2. Two-Dimensional Modeling Studies of Void Linking [with Andrew Geltmacher, Ph.D. Candidate, Dr. Peter Matic, Naval Research Laboratory, and Dr. Michael Stout, Los Alamos National Laboratory]

Our previous experimental modeling studies used primarily Al and brass specimens containing pseudo-random arrays of holes to identify a step-wise, void-linking process. This analysis of void linking depends on the ability of the holes (or voids) to concentrate strain, induce local deformation instabilities and ligament failure, and thereby subsequently promote additional plastic instabilities between neighboring holes.[14,15,17] Void linking is thus viewed as a synergistic process which is very sensitive to void-void interactions and to the presence of void clustering in promoting strain localization, void linking, concentrations, ligament failure and specimen fracture.

While our earlier research on void linking established a physically appealing step-wise linking process which takes into account void microstructures, it relied on crude estimates of strain localization behavior and was confined to uniaxial tension. The present research is intended to make a much more rigorous examination of void linking by utilizing both experiment and computational analysis based on finite element modeling (FEM). We continue to utilize two dimensional modeling so that the "void" linking behavior within a nearly random array of voids can be modeled. In order to make the analysis more general, the present research examines the effects of key parameters such as the strain-hardening capacity of the matrix and the imposed stress state on the process of strain localization between pairs, or groups, of holes and subsequent hole linking. Relying on both experiment and FEM, the research first examines the evolution of stress, strain, and strain energy density states between pairs of hole with differing interhole spacings, matrix strain hardening, and applied stress state (uniaxial or equal biaxial tension). These results not only indicate hole interaction effects and their sensitivity to material flow behavior and stress state but also provide a measure of a multiaxial failure criterion, using the holes to impose the local stress state. The second aspect of our current research extends the above efforts to the hole linking and fracture behavior of specimens containing small arrays (sixteen) of holes. Again, both

computational modeling and experimental validation are being performed as a function of stress state (uniaxial and equal biaxial) and three levels of strain hardening.

In the first part of the study, computer simulation was performed on specimens with pairs of 1.6 mm diameter holes located one, two or three hole diameters apart. The influence of matrix flow behavior was also examined, first, by using the stress-strain curve for 3003 aluminum, which has a strain hardening exponent of $n = d\ln\sigma/d\ln\varepsilon = 0.20$ and, second by assigning the strain-hardening exponents of 0.05 and 0.50 to the matrix material; see Figure 1. It should be noted that all three curves have the same yield stress.

The influence of a geometric defect, such as a pair of holes, on the effective strain distribution is readily apparent in Figures 2 and 4. In Figure 2, the FEM predictions, based on specimens with a strain-hardening exponent n = 0.20, show that (a) the local strains at the mid-plane of the hole (y=0) are ~10 times higher than the applied macroscopic, effective strain of .023 in uniaxial tension (Fig. 2a) but only ~2.5 times larger in equal-biaxial tension (Fig. 2b), and (b) the strain concentration between the holes is more intense in uniaxial tension as compared to equal biaxial tension. Furthermore, other computational results indicate that the above effects (a) and (b) become more pronounced as (1) strain hardening decreases and (2) inter-hole spacing decreases. The first effect is shown in Figures 3a and b, which are the FEM predictions for 1 and 2 hole diameter separation, respectively. This figure is based on specimens with n = 0.20 and an applied macroscopic strain of .01 in uniaxial tension. Figure 3a shows that the local strains at the mid plane are ~75 times larger than the applied strain, whereas Figure 3b these local strains are only ~24 times larger. Also, the strain concentration between the holes is much greater in the smaller hole spacing. Comparison of Figures 4a and 4b shows the effect of the strain-hardening exponent on the local strain concentrations; both Figures are for an applied, uniaxial strain of .01 and a hole spacing of 2 hole diameters. At the mid-plane of the hole, Figure 4a, where n = 0.20, shows that the magnitude of the local strain is ~24 times the applied strain. Whereas, Figure 4b, where n = 0.50, the magnitude of the local strain is only ~7 to 8 times the applied strain. Since ligament failure is strain induced, the "two-hole" computations suggest void linking occurs most rapidly in

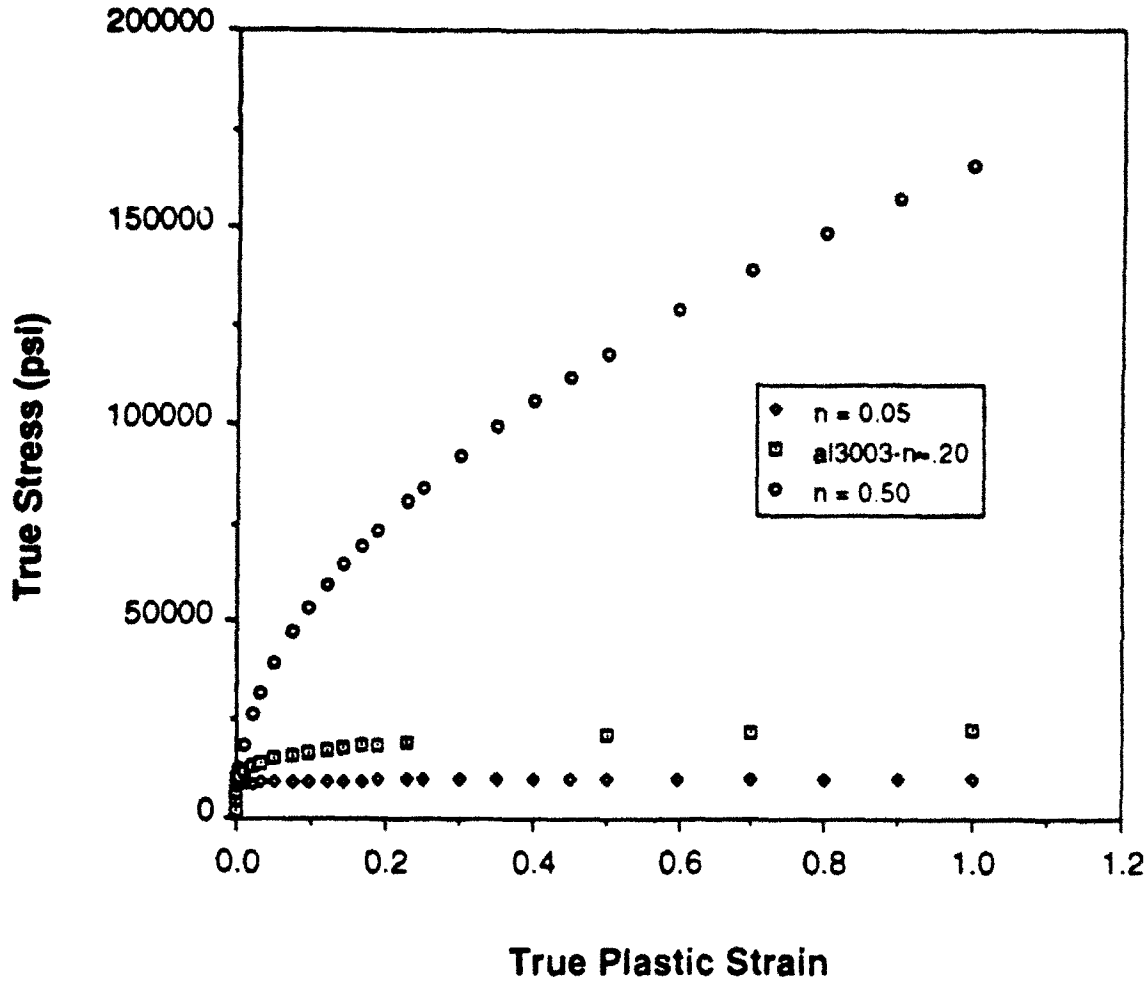

Figure 1. The true stress-strain response used in the computational analyses. The 3003 Al curve is from experimental data while the other stress-strain curves indicate the effect of varying the strain-hardening exponent n as defined by $\sigma = \sigma_0 + k\varepsilon^n$.

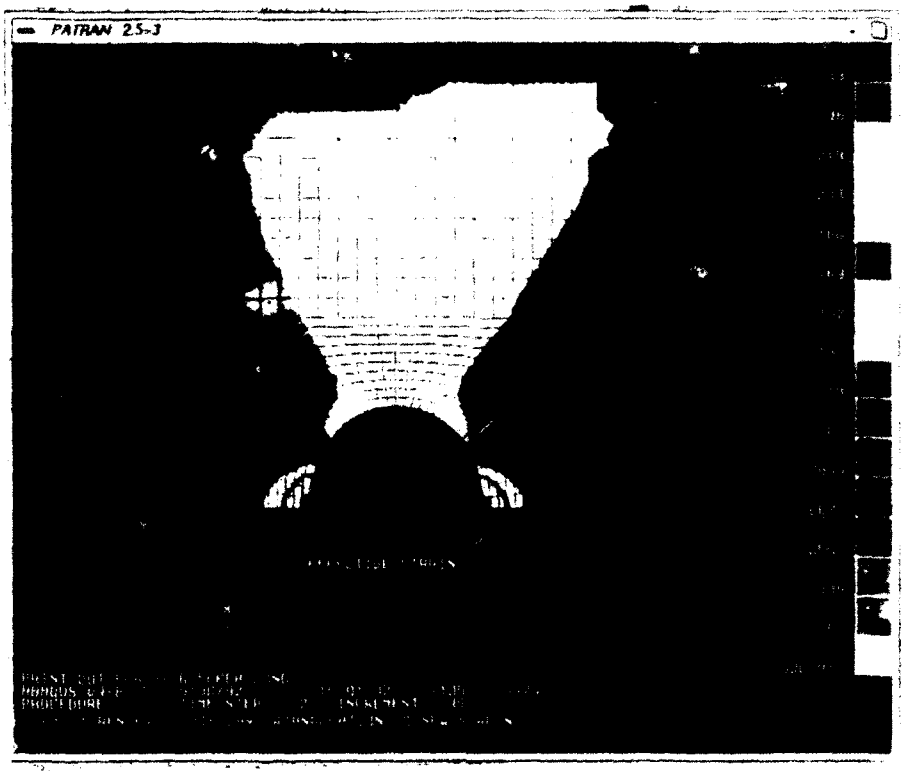

a)

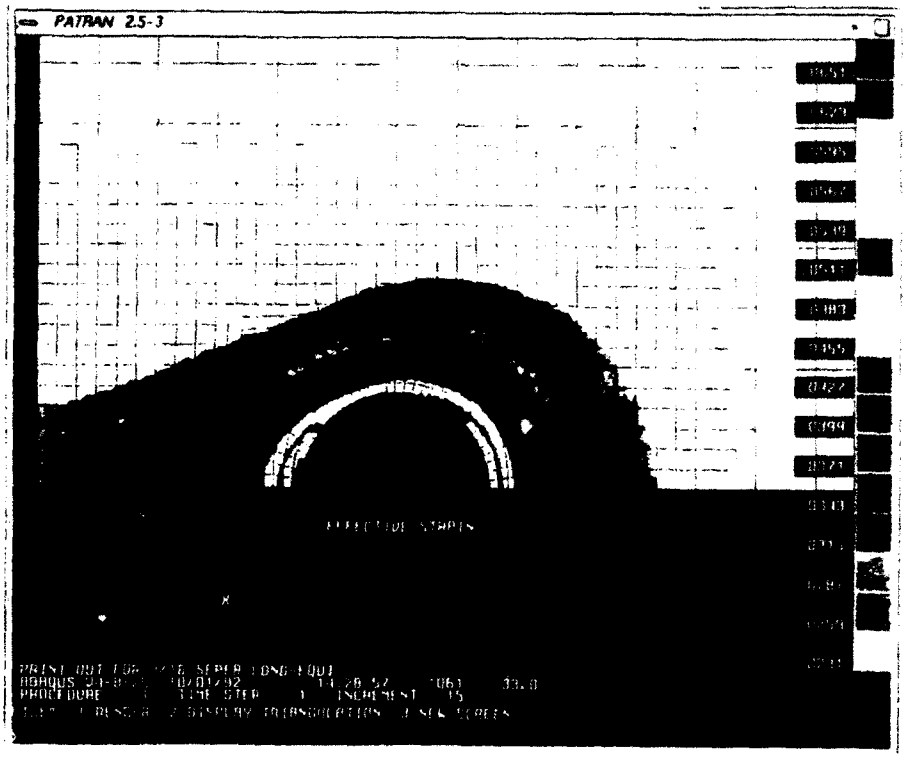

b)

Figure 2. The influence of applied stress state on the effective strain distributions, along the x axis, near a pair of holes spaced three hole diameters apart. The material (n = 0.2) has been deformed in either (a) uniaxial tension in the y direction or (b) equal biaxial tension at an equivalent strain of 0.023 in plane stress. Note differences in strain scales.

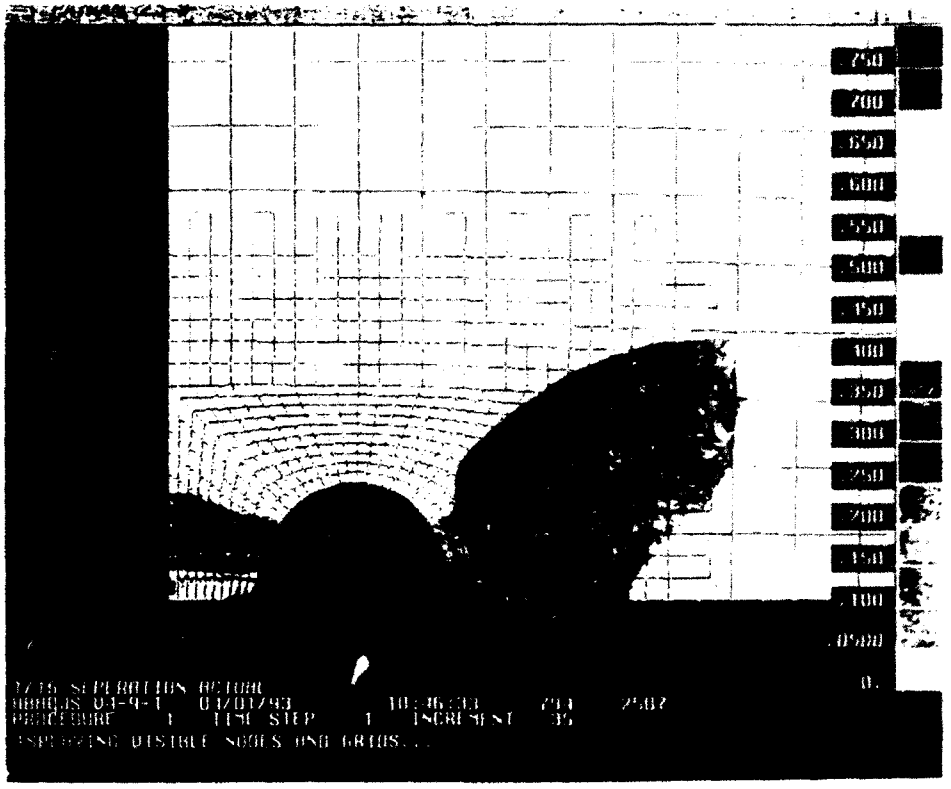

a)

b)

Figure 3. The influence of interhole spacing on the effective strain distributions near a pair of holes located (a) 1 hole diameter apart and (b) 2 hole diameters apart. The material is deformed 0.01 effective strain in uniaxial tension along the y axis; the case is for $n = 0.20$. Note differences in strain scales.

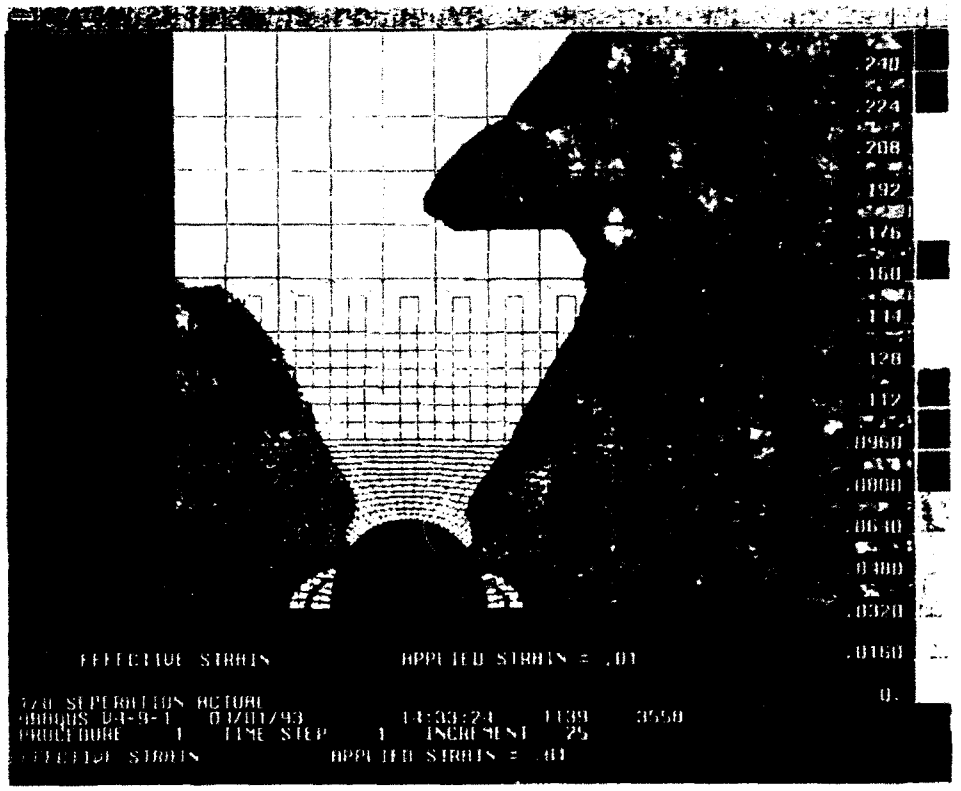

a)

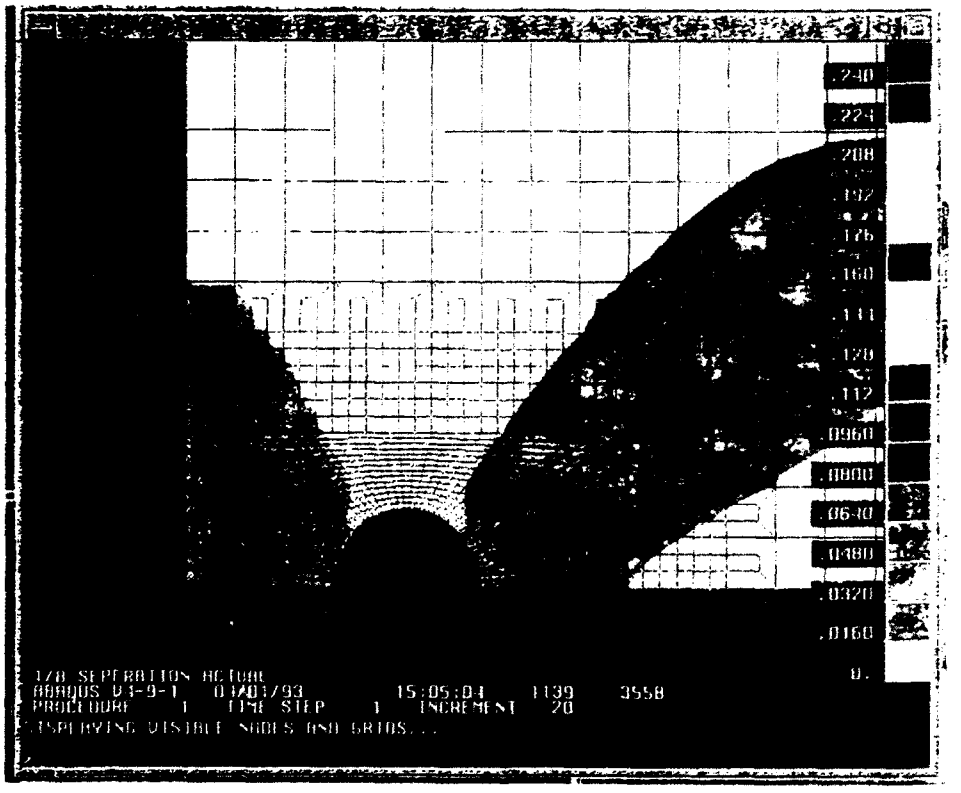

b)

Figure 4. The influence of strain hardening exponent on the effective strain distributions near a pair of holes spaced 2 hole diameters apart in a material with (a) n = 0.20 and (b) n = 0.50 and subjected to uniaxial tension along the y direction to level of 0.01 applied strain.

strain-hardening materials which voids (or holes) are clustered together. This is consistent with our earlier experimental observations.[14]

In the second section of the present work, experimental and computer simulation are used to examine the response of specimens with nearly random arrays of through-thickness holes tested in either uniaxial or equal-biaxial tension. The study relies on specimens containing a sufficient number of holes (16) in order to indicate the behavior of a comparatively realistic hole microstructure. In addition, such a specimen allows us to model the geometry using finite elements under reasonable cost and time considerations. Three 16-hole arrays were generated for the study; the holes have diameters of either 1.6, 3.2 or 4.8 mm. The hole placement was random in a 25 mm diameter target area, subject to the condition that a second hole was not allowed to overlap its nearest neighbor. Figure 5 illustrates the three hole arrays generated. Through the use of both FEM and experiment, these specimens permit a detailed study of not only strain localization and hole linking but also of the multiaxial failure criterion for ligament failure. A determination of this criterion relies on ligaments which have failed as well as those which remain intact. Therefore, a number of data points can be determined from each individual specimen.

The specimen geometry used in the study consisted of uniaxially loaded specimens were 25 cm long (grip-to-grip) and 5 cm wide; see Figure 5. This specimen geometry permits the application of a global uniaxial stress state without dominant interaction effects between the hole array and the edge of the sample. The experiments were performed on HY100 steel specimens of 1.6 or 4.8 mm thickness of (uniaxial tension only) as well as 1 mm thick 3003 Al sheet tested in both uniaxial and equal biaxial tension. The two thicknesses of steel were used in order to observe the effects of out-of-plane constraint on the (i) load/displacement responses, (ii) hole shape changes during deformation, and (iii) the fracture paths of the specimens. The deformation of each specimen was recorded by video tape in conjunction with computer acquisition of the load/displacement data. Computer modeling of the large strain stress-strain response of the matrix materials was performed using the ABAQUS finite element code. PATRAN was used to generate models of all three specimens in two dimensions. The models range from 1328 to 1608 elements

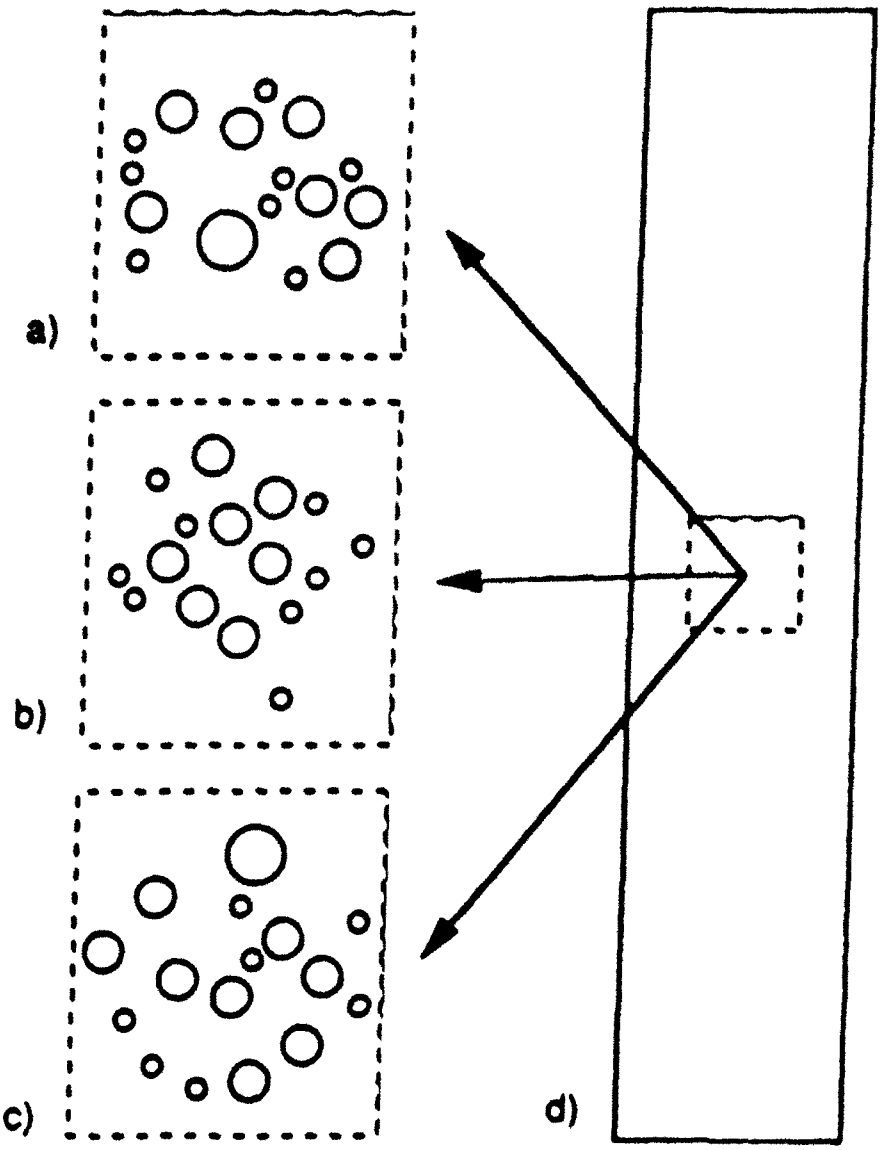

Figure 5. A schematic of the three pseudo random arrays of holes contained in uniaxial tensile specimens analyzed in this study.

for the three specimen geometries. They were analyzed in plane stress and plane strain, and comparison of these solutions are used to examine the effects of out-of-plane constraints on the specimens.

As shown in Figure 6, a comparison of the experimental results and the computational predictions of the plane stress load/displacement responses for each of the multi-hole specimens show very good agreement. The predicted and experimentally determined curves observed exhibit good agreement for each geometry until the load drop in the experimental curve occurs due to crack initiation and growth, as expected. Comparison of the hole shape development up to crack initiation also shows good agreement between experimental and the finite element model, as shown in Figure 7. This agreement includes both the primary and the secondary characteristics of the hole deformation, i.e. the computer simulation predicts the experimentally observed changes of hole shape from circular to either "elliptical", "pear-shaped", or "kidney-shaped". We conclude that the good agreement between the computational predictions and the experimental observations validates the data from the finite element analysis.

As shown in Figure 7a, video images of the deforming specimens indicate regions of high deformation by surface contours. A comparison of the video images to computationally developed strain fields also shows very good agreement with respect to the spatial locations of high deformation. For example, the region of large strain is shaded dark in both the video image and the computations, Figure 6a and 6b, respectively. A very good correlation in positions is seen.

An advantage of the computer model is that it also describes the states of stress, strain and energy densities in the failed ligaments, as well as in those which do not fail. These states, determined from failed and unfailed ligaments, define the upper and lower bounds for the failure criteria of the individual ligaments. This information can then be used to determine a specific criterion for the failure of the ligaments. Therefore, the fracture behavior of specimens with random arrays of holes serve as "multiple test coupons" for the determination of a multiaxial failure criterion for these materials.

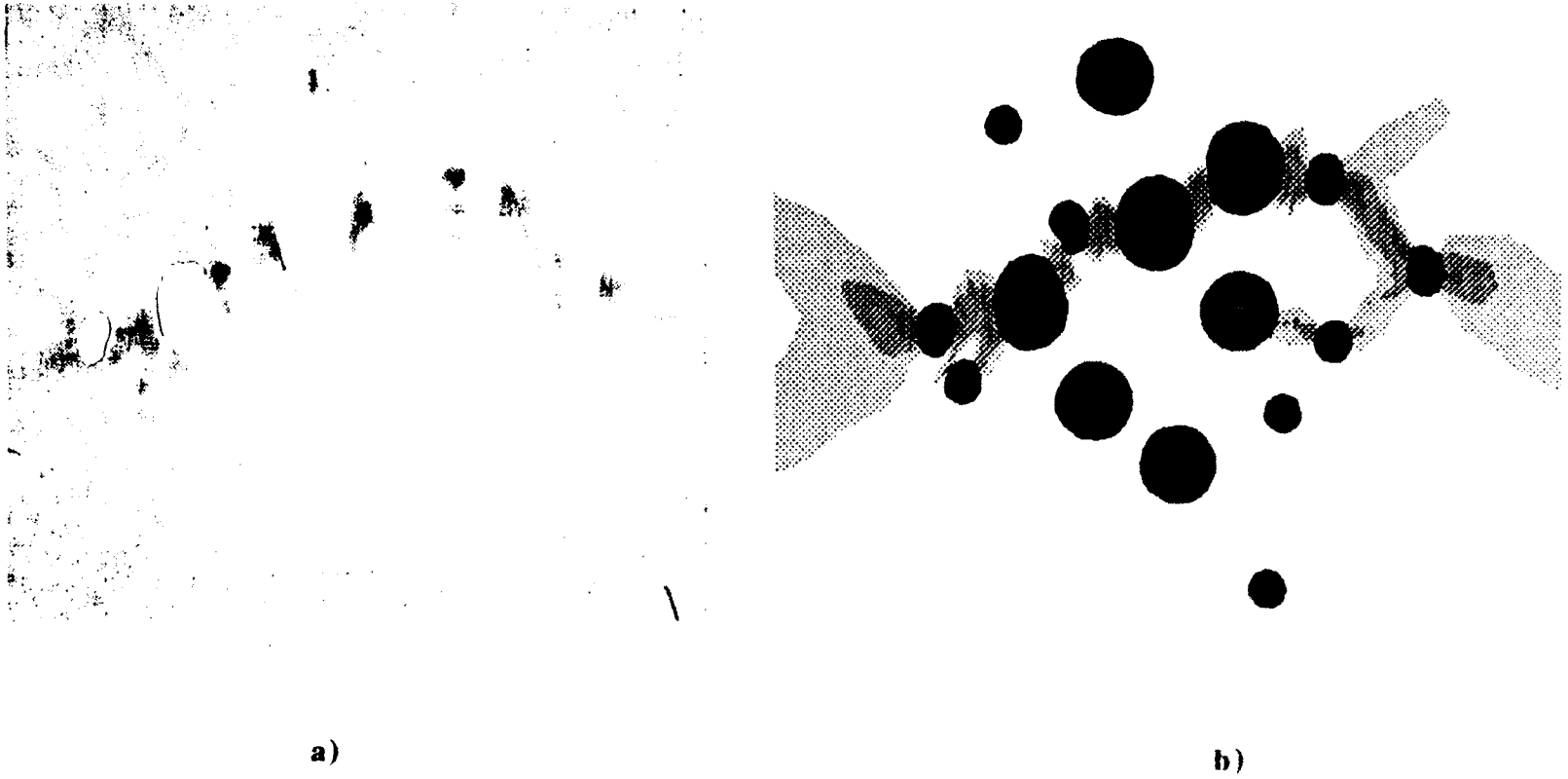

Figure 7. A comparison of strain localization in a 3003 Al specimen containing an array of holes as (a) observed experimentally and (b) predicted computationally.

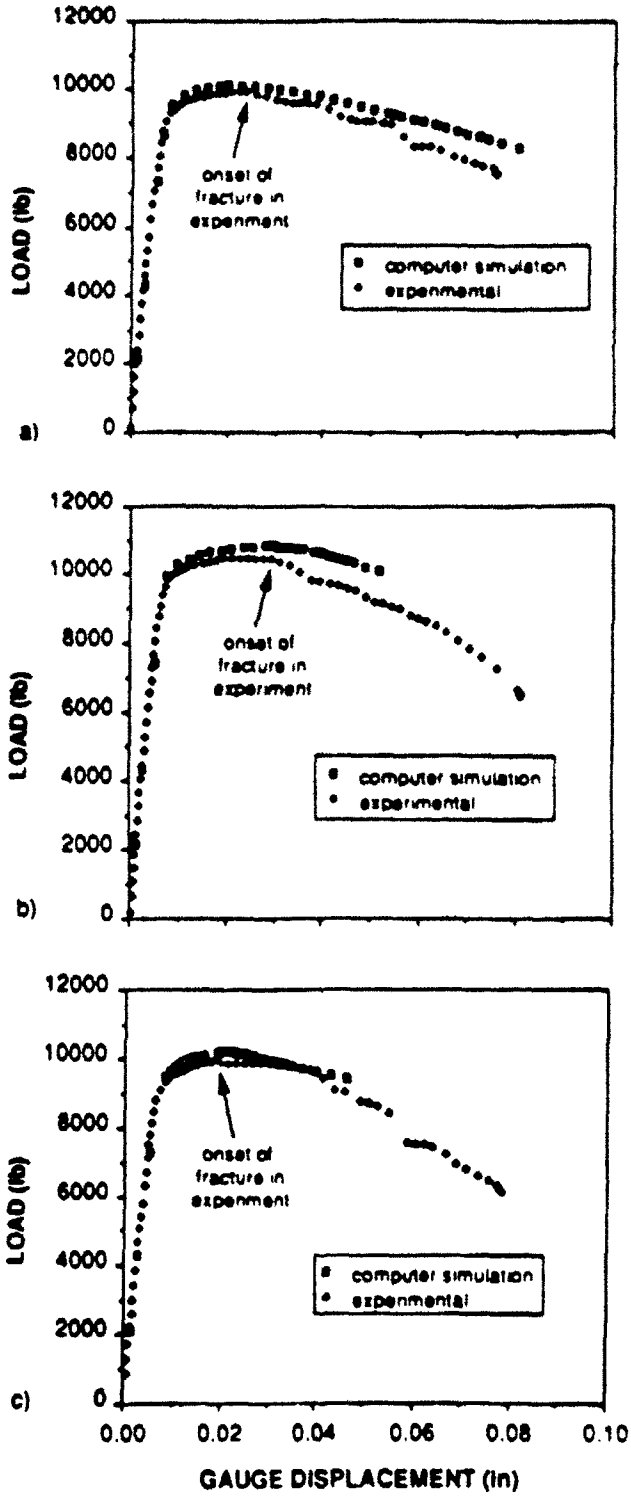

Figure 6. A comparison of computationally predicted and experimentally observed load-displacement responses for tensile specimens containing the hole arrays in Figure 5.

It should be noted that the results of the above study will be presented both at the Canadian Congress of Applied Mechanics (Ottawa, Canada) and at the 25th National Symposium in Fracture Mechanics of ASTM (Lehigh University). The proceedings will be published in a peer-reviewed manner.

Our current efforts have three main thrusts: (1) to complete an examination of the computational predictions of the stress-strain in the vicinity of a pair of holes as a function of interhole spacing, applied strain level, stress state, and strain-hardening exponent, (2) to apply the results of (1) to develop a thorough understanding of the effect of stress state (uniaxial vs. equibiaxial tension) on the experimental observations of hole linking in specimens containing nearly random arrays 63 equi-sized holes in 3003 Al sheets, (3) to complete our computational/experimental analysis of the "16-hole" specimens both with regard to hole linking behavior and the development of multiaxial failure criteria, and (4) to apply (1)-(3) to extending our ability to predict instability-driven void linking phenomena in structural alloys.

3. A Three-Dimensional Experimental Modeling Study of Void Growth and Linking
[with Luis Forero, M.S., January, 1993].

Two-dimensional modeling of void linking provides an important framework for predicting the fracture of structural materials. However, accurate constitutive relationships must be based on three-dimensional (3D) analyses. A reliable analysis for predicting damage-induced ductile fracture must include not only accurate descriptions of void growth and void linking, but also take into account realistic void microstructures. As described earlier in the Background section, it is clear that void interaction effects are important in determining fracture. However, existing 3D computational analyses rely on regular, periodic arrays of spherical, equisized cavities.[3,6,7] While computationally attractive, this is hardly an accurate depiction of a voided material undergoing ductile fracture. Furthermore, the fracture predictions of such computational analyses are suspect. For example, no significant void interaction is predicted for voids spaced one diameter apart in uniaxial tension.[6] This means (a) that void growth to impingement is predicted to occur at

unrealistically large strains[4], (b) that plastic instabilities intervene along long bands of material containing locally high densities of voids (i.e., imperfections),[11-13] or (c) that some arbitrary geometric criterion, which is based on void size-to-spacing ratio, but independent of strain hardening, dictates ligament failure.[17,18] In view of the strong influence of strain hardening on deformation near holes, as described in the previous section, the latter geometric criterion is incomplete at best, while accurate descriptions of imperfections in terms of a "deforming" void microstructure is probably impossible. None of these alternatives are readily applicable to real materials.

An alternate hypothesis is that void interaction effects are actually much stronger than predicted by the computational analyses.[4-8] These predictions are limited to models of periodic arrays of equisized cavities. Is it possible that these[4-8] are inaccurate in predicting even interaction effects between even pairs of closely spaced cavities in a material subjected to uniaxial tension? If so, how accurate are such analyses in predicting void growth and linking near a crack tip? Unfortunately, there are no existing experimental studies which can be used to verify the above computational analyses in a direct manner. Indirect studies which include experiment and computational analysis, such as by Bourcier et al[8], indicate void interactions are more pronounced than are predicted.

The present research project has been recently initiated as an experimental effort (a) to determine the growth behavior of isolated as well as neighboring voids, (b) to identify void interaction effects, and (c) to establish the conditions for void linking,. Although, our initial study is experimental in nature, we hope that the program will shortly evolve to include computational modeling. The present project is based on modeling void interactions between cavities by examining the behavior of tensile specimens containing 1, 2, or 3 cavities. Specimens containing nearly spherical internal cavities have been made by diffusion bonding of pure 18 mm diameter titanium bar at 695°C, 29 MPa pressure for 240 minutes. Nearly spherical cavities, approximately 1 mm diam., created by drilling one end face of the two cylinders, prior to diffusion bonding, as shown in Figure 8. After diffusion bonding, tensile specimens were prepared with the cavities

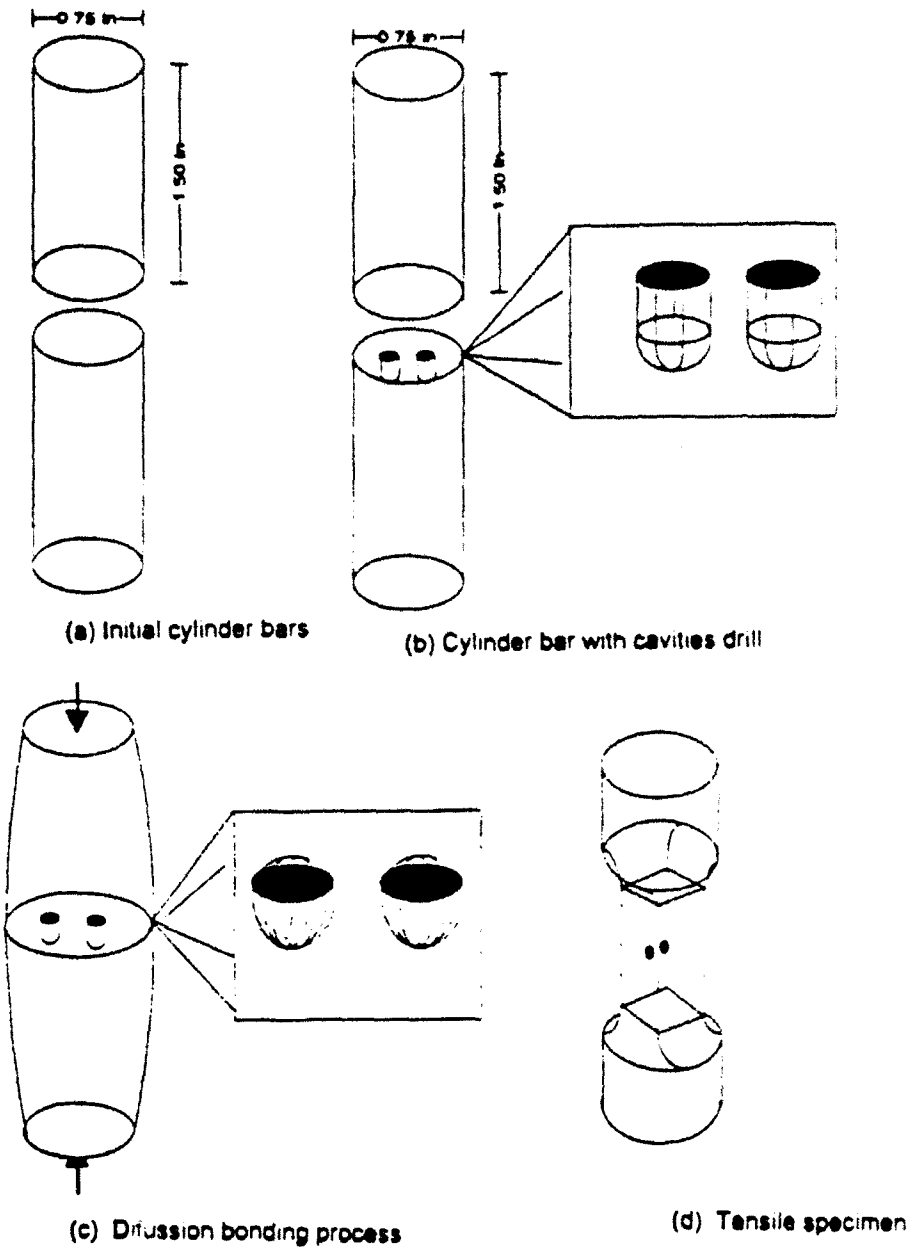

Figure 8. A schematic of the process used to make tensile specimens containing a pair of internal cavities.

centrally located in a gauge section with square 10x10 mm cross section. The diffusion bond line of the test specimens reported contained no porosity and did not bias either deformation or fracture. This specimen geometry permits the monitoring of the cavity growth and linking by interrupting the tensile tests and determining the cavity dimensions generating an ultrasonic C-scan image with a 30 MH_z transducer. Image analysis provides measurements of cavity dimensions to within 0.1 mm.

Tests were successfully performed on seven specimens with cavity configurations shown in Table I. It should be recognized that the entire procedure of specimen preparation and testing is very tedious and time-consuming; for example, the incremental straining plus image analysis of one specimen (as many as 15 steps) would take nearly ten days to complete. The specimens contained either one, two, or three internal cavities, which were located at least three cavity diameters from the specimen surface. Furthermore, the grain size of the Ti matrix was 75μm, which indicates that the intercavity ligament contained from ~6 to ~15 grains. This implies polycrystalline plasticity within the ligament. Since the multiaxial stress fields and large strains near voids in a metal will activate many slip systems even in most single crystals, our model should provide reasonable agreement with ligament deformation behavior between voids in a structural material.

In the initial part of the research, the strain-induced growth behavior of a single, isolated, nearly spherical cavity located internally in titanium tensile specimens has been studied. As shown in Figure 9, the results indicate that the growth behavior of isolated cavities correspond to that predicted by the void growth model of Rice and Tracey[8]. The experimental observations, confirm that for this case, increasing strain causes both the longitudinal cavity dimension and the cavity aspect ratio a/b to increase while the transverse cavity dimension decreases. The void dimension changes linearly with strain, as predicted[8].

The second part of this study analyzes the growth behavior of neighboring cavities, the cavity-cavity interaction effects, and the conditions for the linking of internal cavities for cavities

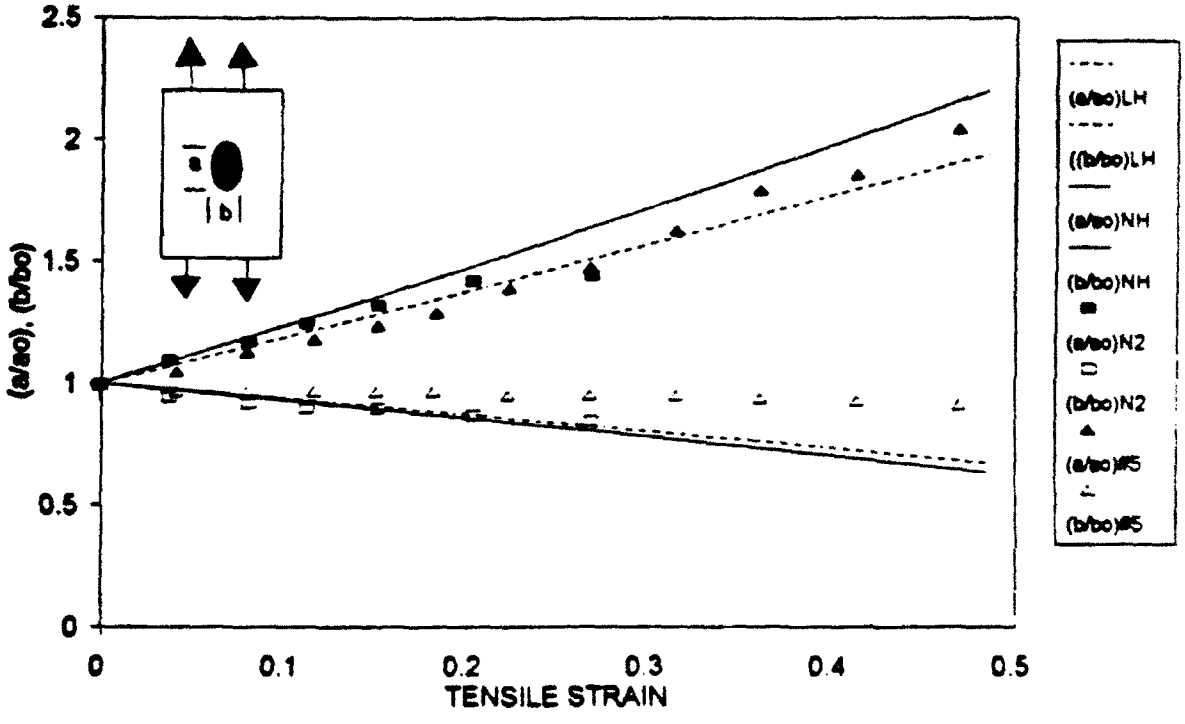

Figure 9. The strain-induced growth of an isolated cavity in a Ti specimen as observed experimentally (data points) and predicted according to the Rice-Tracey analysis for either a non-hardening matrix (solid lines) or a linear hardening matrix (dotted lines).

spaced 0.5 to 2.2 cavity diameters apart. The experimental observations such as in Figures 10-12 provide the following conclusions which are summarized by the schematic in Figure 13:

(a) For intercavity spacings as large as two cavity diameters apart. Both the longitudinal cavity dimension (a/ao) and the transverse cavity dimension (b/bo) increase with increasing strain. As shown in Figures 10-12, this results in a strain-induced decrease of the intercavity spacing as a result of the lateral void growth. Thus, strong void interaction effects occur, even in uniaxial tension.

(b) The lateral cavity growth rates increase with decreasing intercavity spacing.

(c) The presence of a large cavity near a small cavity appears to accelerate the growth of the smaller cavity in both longitudinal and transverse directions. This is shown in Figures 10 and 11, where the smaller cavity #2 grows much faster than cavity #1.

(d) The cavity growth rates are smaller in the transverse axis direction than in the tensile direction, as expected.

(e) Both the longitudinal and the transverse void growth appear to depend roughly linearly on strain. However, there appears to be an acceleration of transverse growth rates at strains of ~0.1 to 0.2. Thus the decrease in ligament width per unit strain appears to accelerate, which suggests the possibility of a plastic instability within the ligament. Optical microscopy of ligament profile after fracture support necking of the ligament, as shown schematically in Figure 13d and 13e.

With reference to void growth and linking during the microvoid fracture of structural materials the following conclusions are suggested by the present initial results:

(a) Void interaction effects definitely occur such that lateral void growth occurs in uniaxial tension. This effect appears to occur for voids spaced as far as two void diameters apart.

(b) The transverse void growth behavior, which results from void-void interaction effects, appears to cause a ligament necking phenomenon. This may be related to a load instability suggested by Thomason.[19,20]

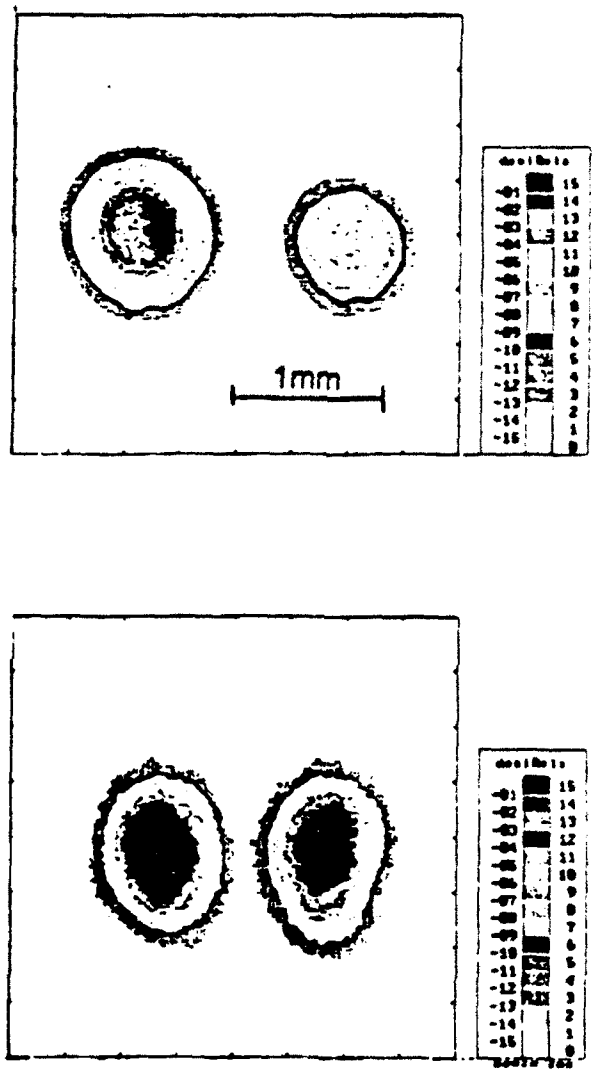

Figure 10. Ultrasonic images of the specimen in Figure 11 taken (a) initially and (b) after a strain of 0.13.

Spec. # 2	a_o (mm)	b_o (mm)	a_o/b_o	d_o (mm)
Cavity #1	0.99	0.94	1.05	0.61
Cavity #2	0.76	0.76	1.00	

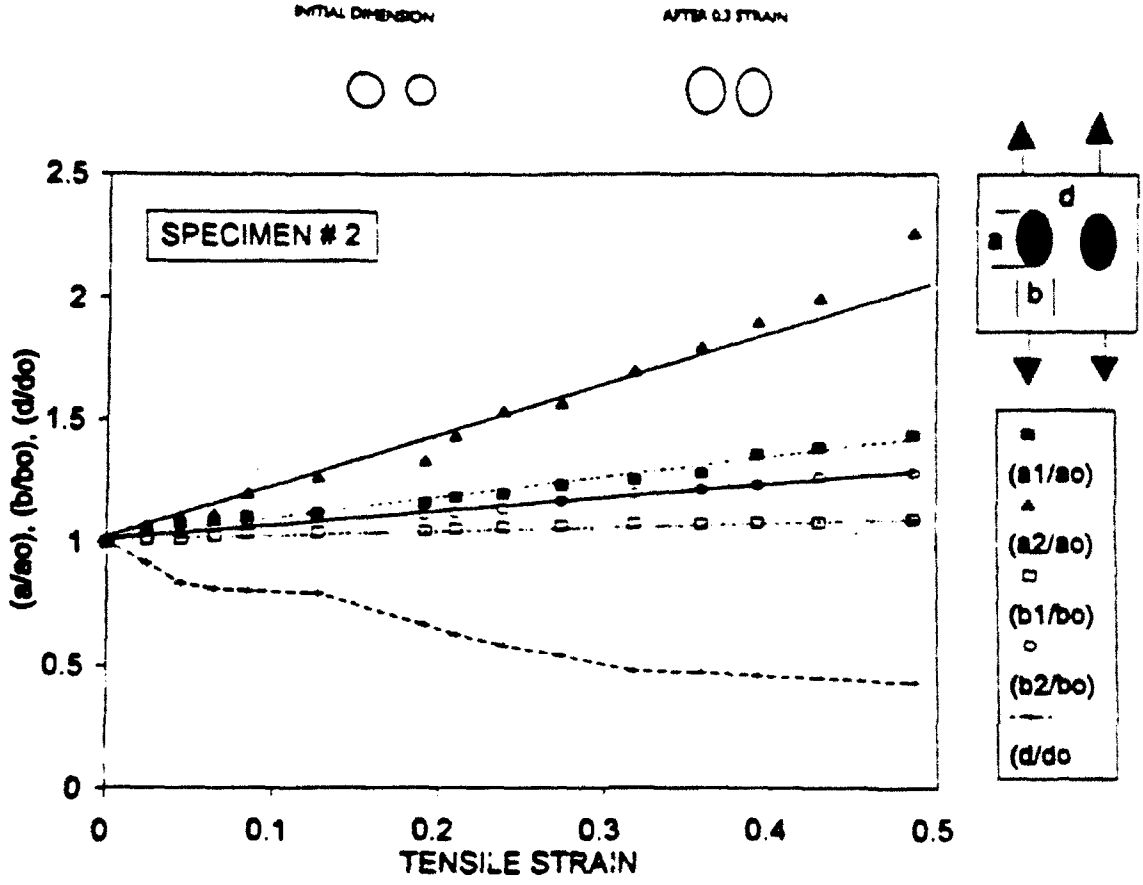

Figure 11. The dependence of cavity growth and interaction on tensile strain for Specimen #2. The specimen fracture strain is 0.55. Note Cavity #2 is smaller and that the cavities are spaced apart 0.6 x Diameter of Cavity #1.

Spec. # 4	a_o (mm)	b_o (mm)	a_o/b_o	d_o (mm)
Cavity #1	1.02	0.89	1.15	0.92
Cavity #2	1.02	0.89	1.15	

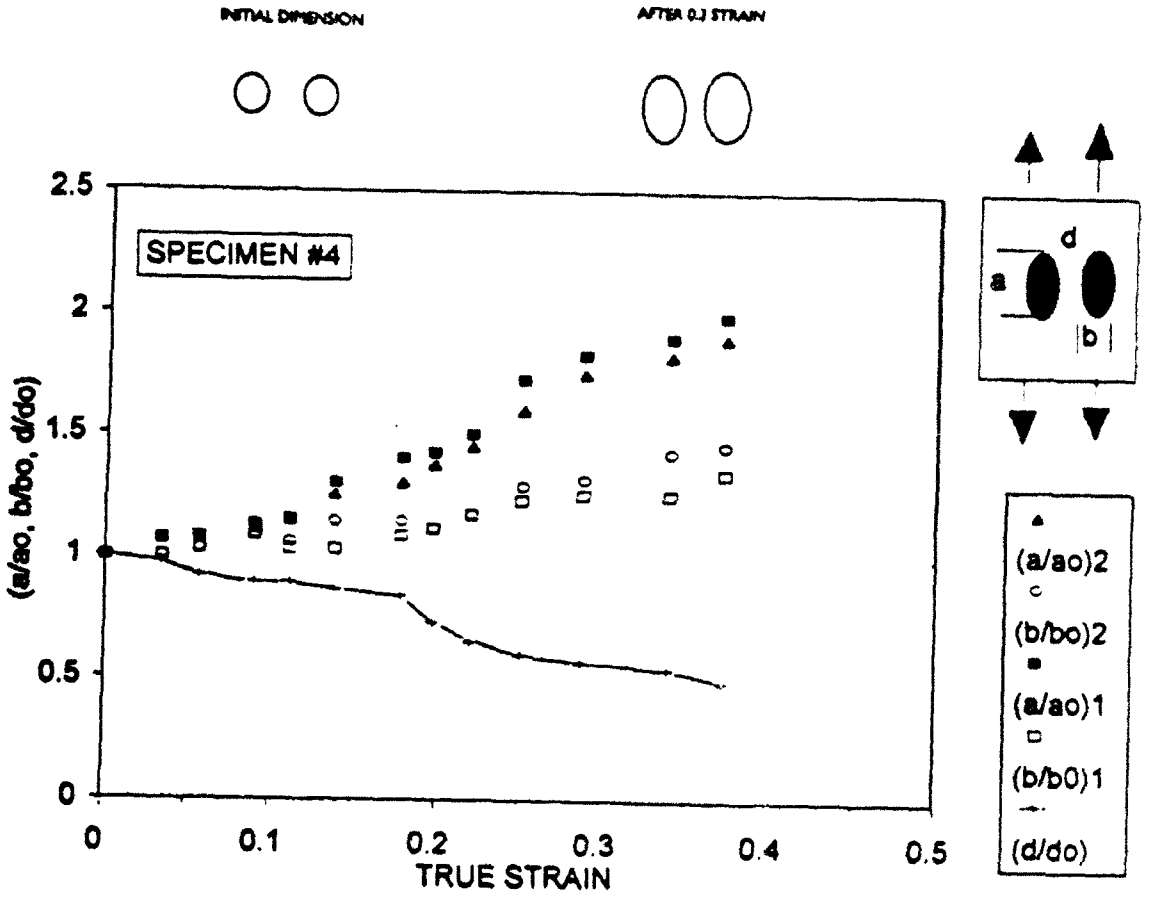

Figure 12. The dependence of cavity growth and interaction on tensile strain for Specimen #4 which contains two equisized cavities spaced 0.9 cavity diameter apart.

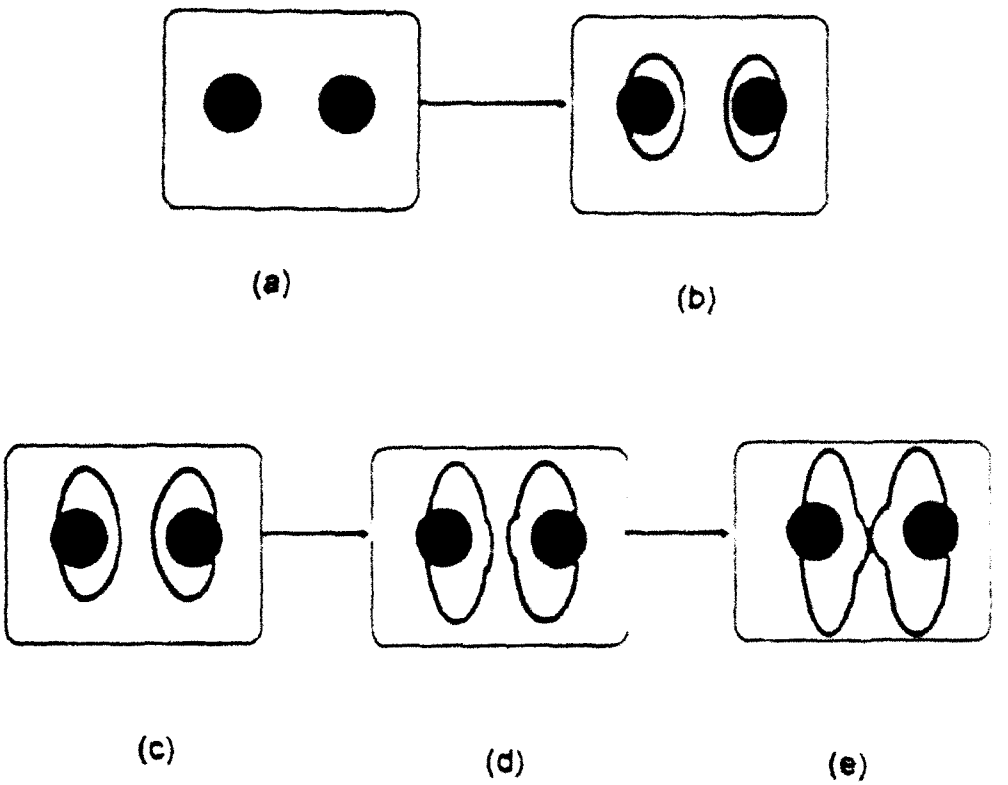

Figure 13. A model of the process of ductile fracture after void nucleation. The initial voids are shown as solid circles.

(c) The combination of (a) and (b) indicate that existing theories for ductile fracture will have much improved predictive capability if they take into account the void interaction and void impingement behavior observed in these experiments.

In summary, these unique experiments raise more questions than they answer. For example, how do we quantify these effects? What is the best method to incorporate the void interactions into ductile fracture theory? How do they depend on the matrix flow behavior or stress state (such as near a crack tip)? Why is there serious disagreement FEM computations? What are the implications of this lack of agreement? We hope to be able to continue this initial effort working with Peter Matic of NRL in the future.

THE INFLUENCE OF TEMPERATURE ON THE DEFORMATION AND OXIDATION BEHAVIOR OF A NEW BETA TITANIUM ALLOY [with Dana Goto, M.S., March, 1993]

Although they possess high strengths at low temperatures, conventional beta Ti alloys usually exhibit poor oxidation resistance and inferior mechanical properties at elevated temperatures. The lack of elevated temperature strength is primarily related to the microstructural instability of the disordered alpha-phase precipitates which harden the matrix, while the poor oxidation resistance is mostly a result of the use of vanadium as the primary beta stabilizing element. The current study is exploring the influence of temperature on the deformation and oxidation behavior of a new beta Ti alloy. Unlike conventional Ti alloys[21], the alloy Ti-23Nb-11Al (at. pct.) [hereafter: Ti-23-11] is strengthened by ordered precipitates based on the alpha-two phase, Ti_3Al. An attractive feature of these precipitates is that they appear to have characteristics suggesting improved thermal stability compared to other high strength beta alloys[21-24]. The absence of vanadium in the Ti-23-11 alloy also suggests enhanced oxidation resistance.

(a) Deformation and Strength Behavior

The temperature dependence of the yield stress for the Ti-23-11 alloy from -196°C to 650°C is shown in Figure 14. In all cases the alloy was solution-treated at 1000°C prior to aging. Figure 14 indicates that (a) age hardening due to alpha-two precipitates results in a very high room temperature yield strength (~1700 MPa); (b) there is a strong temperature dependence of the yield

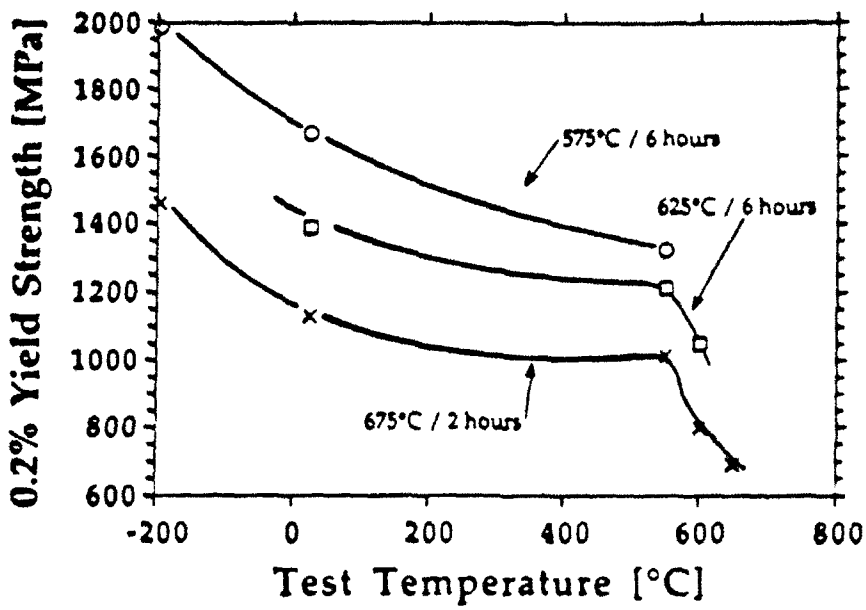

Figure 14. The temperature dependence of the yield strength for the Ti-23Nb-11Al alloy in three age-hardening conditions.

stress below room temperature; (c) most of the room temperature yield strength is retained to ~550°C; and (d) at temperatures greater than 550°C, a rapid decrease in yield strength with increasing temperature can be observed.

The high values of yield strengths possible in this alpha-two strengthened alloy is demonstrated in Figure 15 which compares the specific strengths of Ti-23Nb-11Al to other advanced Ti alloys. Clearly, the present alloy has very attractive specific strength characteristics up to ~550°C.

The large degree of age hardening at room temperature in the Ti-23-11 alloy is obtained despite the fact that there has been no alloy development performed to optimize strength. This is the only alloy of this kind that we have tested. The age hardening response is obviously a result of the relatively small interparticle spacing achievable during the aging treatments as well as the resistance to the shearing of the ordered Ti_3Al-based particles by mobile dislocations[22]. Furthermore, we note that unlike other beta Ti alloys, it is possible to induce very fine, uniform slip, which should results in improved high cycle fatigue resistance, by overaging the alloy at 675°C to induce particle looping.

As shown in Figures 14 and 15, at temperatures greater than ≈550°C, there is a rapid decrease in yield strength with increasing temperature. Nevertheless, for specimens aged 2 hrs at 675°C, roughly 70% of the room temperature yield strength is preserved to 550°C. This is not typical of existing beta-rich alloys which are comparatively much softer (400-600 MPa) in the 550°C temperature range[21]. Thus, as suggested by the relatively good resistance to particle coarsening of the alpha-two precipitate microstructure[25], the resulting age hardening at ~675°C appears to be a relatively effective means of retaining high strengths in beta Ti alloys to the 500-600°C range.

The above observations suggest that the Ti-23-11 alloy has at least short-time precipitate stability at elevated temperatures, up to and including 600°C. However, the stress-strain responses, such as Figure 16 indicate a pronounced tendency for flow softening of specimens aged at 675°C and tested at either 600° or 650°C. Optical microscopy indicates that flow softening is

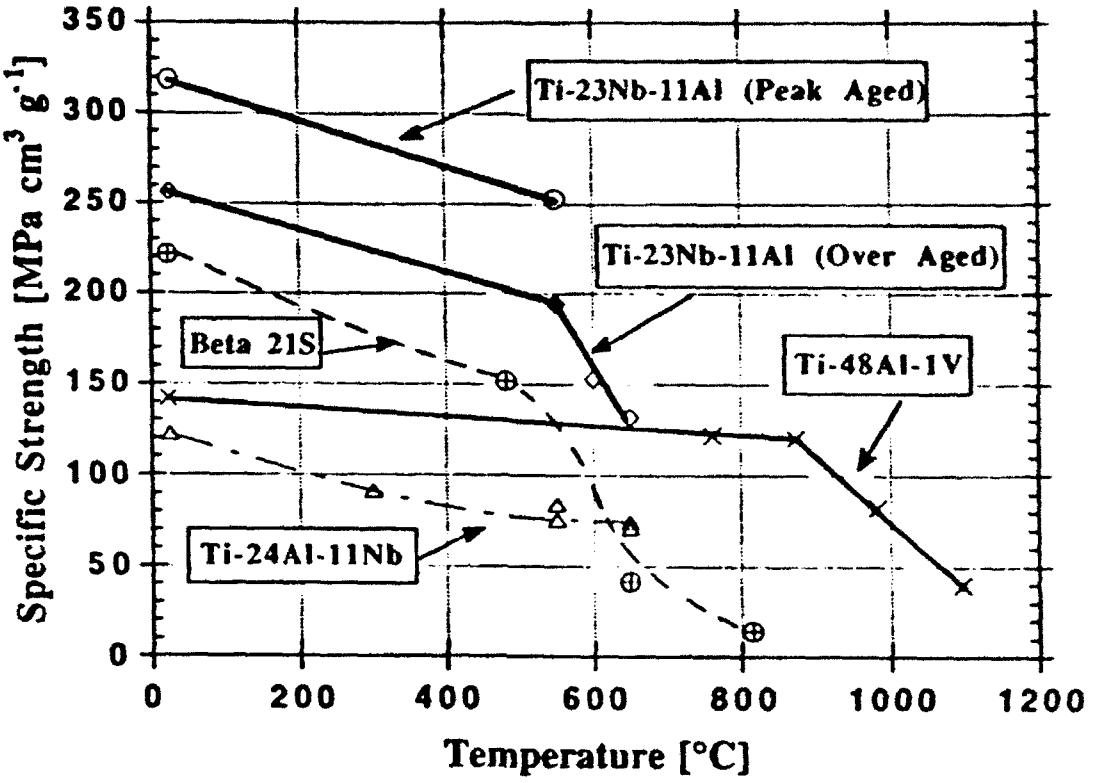

Figure 15. The dependence of specific strength (σ_y/ρ) for Ti-23-11 in the peak-aged condition (575°C/6 hr) and overaged condition (675°C/6 hrs) as compared to beta alloy Beta 21s, the gamma titanium aluminide alloy Ti-48Al-1V, and the alpha-two alloy Ti-24Al-11Nb.

accompanied by the formation of plastic flow localization wherein bands of the microstructure are heavily deformed to create pancake shaped grains with relatively equiaxed bands outside the bands.[24]

The cause of the flow softening phenomena in Figure 16 is not well understood. The present strain rates are too slow for adiabatic heating to be the primary cause. Shear banding similar to that observed above has been observed in alpha + beta Ti alloys and was attributed to the possible generation of a softer crystallographic texture, dynamic recrystallization and/or microstructural coarsening.[26,27] In our case, the relative plastic isotropy of the beta phase minimizes any texture softening effects, and no recrystallization was observed. In addition, microhardness measurements within the shear band indicate hardnesses comparable to the adjacent matrix, suggesting no large loss of hardening. Thus, we infer that the precipitate microstructure appears to be relatively stable. In support of this, we also note that similar flow softening has been observed in solid solution beta-phase Ti-V alloys at 891°C at high levels of V content (25 and 30%).[28] Thus this flow softening phenomenon in Figure 16 appears to be a characteristic of deformation dynamics behavior within the solid solution matrix and not of specific dislocation-precipitate interactions.

The relationship between flow stress and strain rate was examined between 550°C to 650°C and strain rates of $3x10^{-4}s^{-1}$ to $10^{-2}s^{-1}$. Very large ($n>40$) stress exponents, $n = d\ln\dot{\varepsilon}/d\ln\sigma$, were observed in all cases indicating that dislocation glide-controlled processes still dominate deformation. This is not surprising considering that 650° is about 0.5 T_{MP}, and most of the data are consistent with the Sherby and Burke[29] observation that power law breakdown creep occurs whenever $\dot{\varepsilon}/D_L \geq 10^{13}$ m,$^{-2}$ where D_L is the self diffusion coefficient of the β Ti matrix.[30] Testing at temperatures higher than 650°C and at much lower strain rates was precluded by precipitate instability, while the pronounced flow softening discouraged attempts to obtain steady state creep behavior at constant stress through slow strain-rate compressive creep techniques.

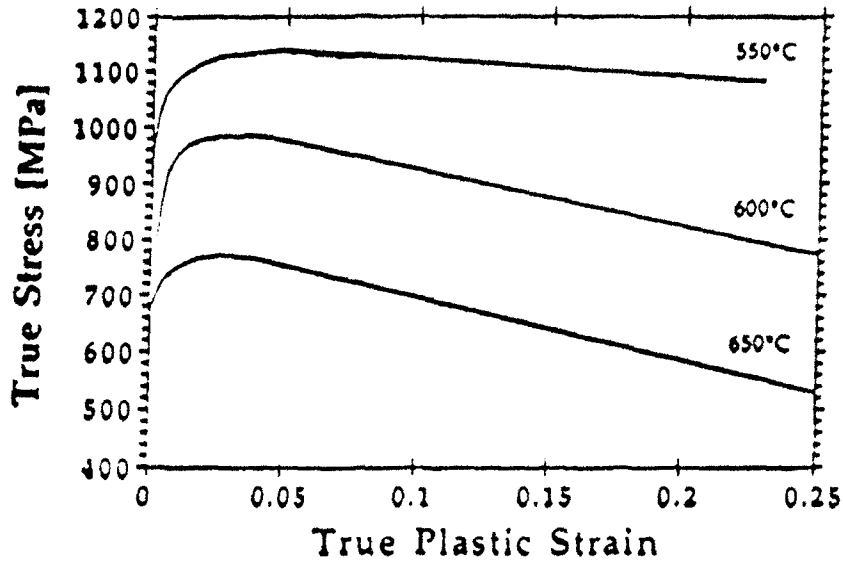

Figure 16. Stress-strain responses for Ti-23-11 at 550°C exhibiting zero strain-hardening conditions, and at 600 and 650°C, respectively, exhibiting flow softening (negative strain-hardening). Specimen was solution-treated and aged at 675°C for 2 hrs.

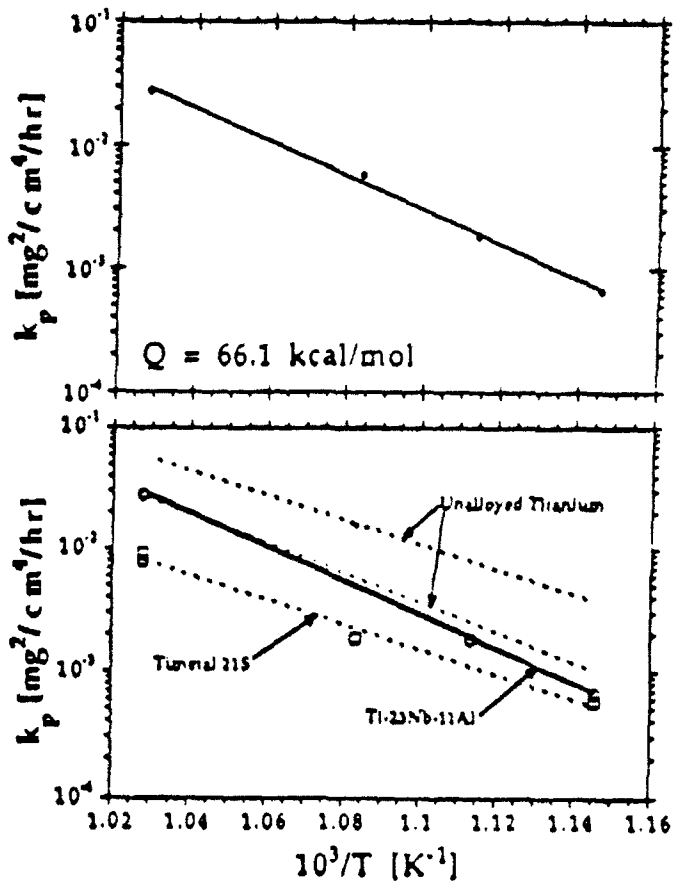

Figure 17. Arrhenius plot of parabolic rate constants for (a) Ti-23-11 oxidized in laboratory air between 600 and 700°C for up to 96 hours. Also included in (b) are the parabolic rate constants for Ti-15Mo-2.7Nb-3Al-0.2Si (Timetal 21S), after ref. 33, and unalloyed titanium, after ref's 34 and 35.

(b) Oxidation Behavior

In addition to creep resistance, the oxidation resistance of titanium alloys is a primary issue regarding their elevated temperature applicability. Beta titanium alloys generally possess poor oxidation resistance, due in part to the presence of the beta-phase stabilizing elements such as vanadium.[31] Recently, replacing vanadium by molybdenum (as the β-phase stabilizer), has improved the oxidation resistance of the β-titanium alloy, Timetal 21S.[31] In the present case, it should be recalled that Ti-23-11 contains a significant amounts of Nb and Al but no V.

The weight-gain behavior of the Ti-23-11 oxidized in flowing laboratory air over the temperature range of 600° to 700°C for times up to 96 hours exhibits parabolic oxidation kinetics, such that weight gain during oxidation may be expressed by the relationship

$$m = \sqrt{k_p t} \qquad (2)$$

where m is the weight gain per unit area of original sample, k_p is an effective parabolic rate constant, and t is the time of exposure at the oxidation condition. The continuously increasing sample weight with increasing time implies that a protective oxide scale does not form within the exposure times examined. Furthermore, the Ti-23-11 did not exhibit gross discontinuities in weight gain during oxidation; i.e. no gross transitions in oxidation kinetics were recorded by the thermogravimetric analysis (TGA) equipment. This suggests single stage parabolic oxidation kinetics with no significant changes in the dominant oxidation mechanism over the temperature range and exposure times investigated.

Assuming the oxidation process to be diffusion controlled, as shown in Figure 17, the TGA data of can be analyzed in the form of an Arrhenius-type relationship such that the effective parabolic rate constant for Ti-23-11 is

$$k_p = 2.37 \times 10^{13} \exp\left(\frac{-66\,102}{RT}\right). \qquad (21)$$

The activation energy for oxidation (Q = 66 kcal/mol or 277 kJ/mol) obtained from Equation 2 corresponds reasonably well with literature values (Q = 250 - 300kJ/mol) for oxidation of titanium.[32] Consistent with that behavior, this result tends to indicate that oxidation is rate controlled by oxygen diffusion through a scale.

Inspection of oxidized material (exposed at 600°C for 48 hours) revealed a scale of thickness on the order of ≈1 μm. This is similar to the oxide thickness (≈ 0.8 μm) which was observed in the oxidation resistant β-titanium alloy, Timetal 21S, (Ti-15Mo-2.7Nb-3Al-0.2Si) which was exposed at 600°C for 72.5 hours in air.[33]

Finally, Figure 17b also shows a comparison of the parabolic rate constants for the Ti-23-11 alloy with a range of literature values for pure Ti as well as data for the "oxidation-resistant" beta alloy Timetal 21S. The results indicate the Ti-23-11 to be somewhat better than pure Ti. When compared to Timetal 21S, the Ti-23-11 alloy shows similar oxidation behavior in air at 600°C, but it is worse at 700°C.

(c) Fracture Behavior

We are currently examining the tensile ductility of this high strength Ti alloy. At a peak yield strength (aged that 575°C), preliminary tests indicate ductility of ~1% accompanied by slip band decohension due to the coarse planar slip. We are currently trying to use step aging as a means of obtaining a better combination of high strength and ductility. Specifically, aging at low temperatures to nucleate a high density of closely spaced precipitates is being followed by a high temperature (675°C) aging treatment to grow the particles to a size large enough to cause dislocation looping, which should improve ductility, but to preserve small interparticle spacings for strength.

D. Summary

This study establishes the concept that, despite the absence of any alloy development, the beta Ti alloy, Ti-23Nb-11Al, can be age-hardened by α_2-phase precipitates to a high level of strength. Furthermore, the ordered precipitates exhibit comparatively good resistance to particle coarsening phenomena, thus providing at least short-time strength retention to temperatures of ~600°C, which is much higher than conventional β Ti alloys. In this temperature range, the Ti-23-11 has similar oxidation resistance in flowing air to the recently developed Timetal 21S. Our

current efforts are designed to complete this project by exploring heat treatments designed to optimize a combination of high strength and tensile ductility.

REFERENCES

1. A. R. Rice and D. M. Tracey, J. Mech. Phys. Solids, 17, 201 (1969).
2. B. Budiansky, J. W. Hutchinson and S. Slutsky in Mechanics of Solids (Pergamon Press, Oxford), 1982, p. 13.
3. C. J. Worswick and R. J. Pick, J. Mech. Solids 38, 601 (1990).
4. D. M. Tracey, Eng. Frac. Mech. 3, 301 (1971).
5. E. Needleman, J. Appl. Mech., 39 (964) 972.
6. F. L. Hom and R. M. McMeeking, J. Appl. Mech. 56, 309 (1989).
7. G. Tvergood, Int. J. Fracture, 17, 389 (1981).
8. R. J. Bourcier, D. A. Koss, R. E. Swelser and O. Richmond, Acta Metall. 34, 2443 (196).
9. I. L. Hom and R. M. McMeeking, J. Mech. Phys. Solids, 37, 395 (1989).
10. J. M. McMeeking and C. L. Hom, Int. J. Frac. 42, 1 (1990).
11. K. Yamamoto, Int. J. Frac., 141, 347 (1978)
12. L. Sage, J. Pan and A. Needleman, Int. J. Frac. 191, 153 (1982).
13. M. Ohno and J. Hutchinson, J. Mech. Phys. Solids, 321. 63 (1984).
14. P. E. Magnusen, E. M. Dubensky and D. A. Koss, Acta Met 36, 1503 (1988).
15. P. E. Magnusen, D. J. Srolovitz and D. A. Koss Acta Met 38, 1013 (1990).
16. P. F. Thomason, Acta Metall. 33, 1095 (1985).
17. L. M. Brown and J. D. Embury in Proc. 3rd Int. Conf. on Strength of Metals and Alloys, 1973, p. 164.
18. G. LeRoy, J. D. Embury, G. Edward, and M. F. Ashby, Acta Metall. 29, 1509 (1981).
19. P. F. Thomason, Acta Metall. 29, 763 (1981).
20. P. F. Thomason, Acta Metall. 30, 279 (1982).
21. Beta Titanium Alloys in the 1980's, R. R. Boyer and H. W. Rosenberg, eds. (Warrendale, PA: TMS, 1984).
22. L. S. Quattrocchi, D. A. Koss, and G. Scarr Scripta Metall. et Mater, 26 (1992) 267.

23. L. S. Quattrocchi and D. A. Koss, in Proc. to Seventh World Conf. on Titanium, San Diego, 1992.

24. D. Goto, L. S. Quattrocchi, and D. A. Koss, to be published in Titanium '94 (TMS, Warrendale), 1993; see also Tech. Rep. No. 5, ONR Grant No. N00014-91-3-14 14, March, 1993.

25. R. D. Doherty, Met. Sc. 16, (1982) 675.

26. P. Dadros and J. F. Thomas, Metall. Trans., 12A (1981) 1867.

27. S. L. Semiatin and G. D. Lahoti, Metall. Trans., 12A (1981) 1705.

28. H. Oikawa in Creep and Fracture of Engineering Materials and Structures, ed. by B. Wilshire and R. W. Evans (London, Inst. of Metals, 1991), p. 31.

29. O. D. Sherby and P. M. Burke, Prog. Mater. Sci., 13 (1967) 325.

30. H. Oikawa, K. Nishimura and M. X. Cui, Scripta Metall., 19 (1985) 825.

31. P. J. Bania, ISIJ Int., 31 (1991) 840.

32. Z. Liu and G. Welsch, Metall. Trans. A, 19A (1990) 1121.

33. T. A. Wallace, R. K. Clark and K. E. Wiedemann in Seventh World Conf. on Titanium.

34. A. M. Chaze and C. Coddet, J. Less Common Met. 157 (1990) 55.

35. J. Unnam, R. N. Shenoy, and R. K. Clarke, Oxid. Met. 26 (1986) 231.